Electronic Supplementary Information for:

High-Performance See-Through Power Windows

Di Wang[a], Yuhao Li[b], Guanqing Zhou[c], Emely Gu[d], Ruoxi Xia[e], Buyi Yan[d], Jizhong Yao[d], Haiming Zhu[c], Xinhui Lu[b], Hin-Lap Yip[e,f], Hongzheng Chen[a], Chang-Zhi Li[a,*]

[a]State Key Laboratory of Silicon Materials, MOE Key Laboratory of Macromolecular, Synthesis and Functionalization, Department of Polymer Science and Engineering, Zhejiang University, Hangzhou 310027 (P. R. China)

[b]Department of Physics, Chinese University of Hong Kong, New Territories, Hong Kong, 999077 (P. R. China)

[c]Department of Chemistry, Zhejiang University, Hangzhou 310027 (P.R. China)

[d]Microquanta semiconductor, Hangzhou 311121 (P. R. China)

[e]State Key Laboratory of Luminescent Materials and Devices School of Materials Science and Engineering South China University of Technology Guangzhou 510640 (P. R. China)

[f]Department of Materials Science and Engineering, City University of Hong Kong, Tat Chee Avenue, Kowloon, Hong Kong, 999077 (P. R. China)

*Email: czli@zju.edu.cn

Materials and Methods

Device Fabrication: Organic solar cells were fabricated on indium tin oxides (ITO) glass substrates with the structure of ITO/PEDOT: PSS-TA/active layer/Bis-FIMG/Ag. The glass/ITO substrates were cleaned by sonication using detergent, deionized water, acetone, and isopropanol sequentially for 30 min before fabrication. The PEDOT: PSS-TA is prepared by adding the same amount of deionized water to PEDOT:PSS (Baytron P AI4083, 1:1 vol) and adding tyramine (TA) at 0.7mg/ml. The pre-cleaned ITO substrates were then treated in an ultraviolet generator for 30 min, followed by the deposition of PEDOT: PSS-TA thin film (10nm) and then annealing at 150℃ for 30 min. Then the substrates were transferred into a glovebox. The PM6: acceptors active layers (D:A = 1:1.2 weight ratio for binary, and the miscible BO-4Cl and m-BTP-PhC6 stand for acceptors in ternary) were then spin-coated from 17.5 mg/mL chloroform solution with 0.4 vol.% 1-chloronaphthalene (CN) for ternary blend and PM6: m-BTP-PhC6 binary blend and with 0.25 vol.% 1,8-diiodooctane (DIO) for PM6:BO-4Cl binary blend, at 3500 rpm for the 30s to form an active layer of around 100 nm. And then the half-finished devices were annealed at 85 ºC for 8 min. The Bis-FIMG layer was deposited from 1 mg/mL of methanol solution at 3800 rpm for the 40s. Ag electrode with a suitable thickness (100 nm) was deposited by thermal evaporation under a background pressure of approximately 1.5×10^{-4} Pa, to complete the device with an 5.979 mm^2 mask (credentialed by the National Institute of Metrology (NIM), Beijing). **Semitransparent OSCs** were fabricated by following the same procedure while adjusting the active layer to around 70 nm. Then the 16 nm ultra-thin silver is evaporated atop of Bis-FIMG ETL. DBR structure (MoO_3/ LiF/ MoO_3) is deposited on top of ultra-thin silver under a background pressure of approximately 1.5×10^{-4} Pa. The area of the active layer for semitransparent organic solar cells is 4 mm^2.

Organic solar modules Glass substrates (6×6 cm^2) are provided with pre-deposited ITO layer. The film stack is laser scribed by a 1064 nm nano-sec beam (2 W) to form isolated cell units. PEDOT: PSS-TA thin film (10nm) layers were prepared by following the same procedure as fabricating small area devices. Then the substrates were transferred into a glovebox. The ternary blends (PM6: BO-4Cl :m-BTP-PhC6, 1:0.36:0.84, by wt%) were spin-coated in 17 mg/ml of chloroform solution with 0.4 vol.% 1-chloronaphthalene (CN) at the speed of 2800 rpm for 30s to obtain ~100 nm active layer. And then the half-finished devices were annealed at 85 ºC for 8 min. The Bis-FIMG layer was deposited from 1 mg/mL of methanol solution at 3800

rpm for the 40s. A 532 nm nano-sec laser beam (2W) is used for P2 scribing to expose the top ITO layer for later series connection. Ag electrode is vacuum deposited to finalize the module layer stack. P3 scribing and P4 edge isolation are carried out with the same 532 nm nano-sec beam (2 W).

Solar cell characterization: The current density-voltage (*J-V*) curves of OSCs were measured in the glovebox with Keithley 2400, under AM 1.5G illumination at 100 mW cm^{-2} irradiation using an Enli SS-F5-3A solar simulator, and the light intensity was calibrated with a standard Si solar cell with KG2 filter (made by Enli Technology Co., Ltd., Taiwan, and calibrated report can be traced to NREL). The EQE spectrum was measured using a QE-R Solar Cell Spectral Response Measurement System (Enli Technology Co., Ltd., Taiwan).

Solar module characterization: The *J-V* characteristic curves of modules were recorded on the Keithley source unit 2400 under AM 1.5G 1 sun intensity illumination (100 mW/cm^2) by a AAA solar simulator (SS-100A) from Beijing Sanyou Technology, and the light intensity was calibrated with a standard photovoltaic reference cell. *J-V* scan speed and dwell time are 0.02 V/step and 1 ms, respectively. The *J-V* measurements of modules were performed in a glovebox under N_2 atmosphere with the mask (19.30 cm^2 full open area, no shade in interconnection area). Organic modules were measured by the Chinese National Photovoltaic Industry Metrology and Testing Center (NPVM) with an 18.61 cm^2 mask for performance certification.

Transient Absorption Spectroscopy: For femtosecond transient absorption spectroscopy, the fundamental output from Yb: KGW laser (1030 nm, 220 fs Gaussian fit, 100 kHz, Light Conversion Ltd) was separated into two light beams. One was introduced to NOPA (ORPHEUS-N, Light Conversion Ltd) to produce a certain wavelength for the pump beam (here we use 750 nm), the other was focused onto a YAG plate to generate a white light continuum as the probe beam. The pump and probe overlapped on the sample at a small angle of less than 10°. The transmitted probe light from the sample was collected by a linear CCD array. Then we obtained transient differential transmission signals by the equation shown below:

$$\frac{\Delta T}{T} = \frac{T_{\mathrm{pump-on}} - T_{\mathrm{pump-off}}}{T_{\mathrm{pump-off}}}$$

Time-resolved Photoluminescence Spectroscopy: The optically pumped lasing measurements were taken on a home-build far-field microfluorescence system (Olympus, IX73 inverted microscope). The excitation light (515 nm) was generated from the second harmonic of the fundamental output that was seeded by a mode-locked Ti: sapphire laser (Light Conversion Pharos, 1030 nm, < 300 fs, 1 MHz). The excitation light was filtered with a 515 nm band-pass filter and then diverged with a convex lens (f = 500 mm), finally focused down to a 140 μm diameter spot through an objective lens (Olympus MplanFLN, 20x, NA = 0.45). The emission light was collected by the same objective and focused on a spectrograph (Princeton Instruments, Acton SpectraPro, SP-2300i) with a 600 mm^{-1} grating and detected by a liquid-N_2-cooled CCD. The instrument resolution (FWHM) was ~0.1 nm. All measurements were taken at room temperature with pulse picker = 1000. TRPL decay kinetics were collected using a TCSPC module (PicoHarp 300) and a SPAD detector (IDQ, id100) with an instrument response function ~100 ps.

SCLC Measurements: The charge carrier mobilities of the blend films were measured using the space-charge-limited current (SCLC) method. Hole-only devices were fabricated in the structure of ITO/PEDOT: PSS-TA/active layer/MoO_3/Ag, electron-only devices were fabricated in the structure of ITO/ZnO/active layer/Bis-FIMG/Ag. The device characteristics were extracted by modeling the dark current under forwarding bias using the SCLC expression described by the Mott-Gurney law:

$$J = \frac{9}{8}\varepsilon_r \varepsilon_0 \mu \frac{V^2}{L^3}$$

Here, $\varepsilon_r \approx 3$ is the average dielectric constant of the blend film, ε_0 is the permittivity of the free space, μ is the carrier mobility, $L \approx 100$ nm is the thickness of the film, and V is the applied voltage.

GIWAXS Measurements: Silicon wafers (thickness 625±25 μm) were first ultrasonicated in ethanol for half an hour. After UV-ozone treatment for 10 min, it was transferred into a glove box for coating of blend films. The PM6: acceptors (D:A) was fixed to 1:1.2 weight ratios for binary and ternary (the miscible BO-4Cl and m-BTP-PhC6 stand for acceptors) blends. Sample films around 80 nm were then spin-coated from 17.5 mg/mL chloroform solution with 0.4 vol.% 1-chloronaphthalene (CN) for ternary blend and PM6: m-BTP-PhC6 binary blend, and solution with 0.25 vol.% 1,8-diiodooctane (DIO) for PM6:BO-4Cl binary blend, at

3500 rpm for the 30s. And then the sample films were annealed at 85 ^{o}C for 8 min. Grazing-incidence wide-angle and small-angle X-ray scattering (GIWAXS/GISAXS) measurements were carried out with a Xeuss 2.0 SAXS/WAXS laboratory beamline using a Cu X-ray source (8.05k eV, 1.54 Å) and a Pilatus3R 300K detector. The incidence angle is 0.2^{o}.

AFM characterization: Topographic and phase images of films were obtained on a VeecoMultiMode AFM in the tapping mode, and the scanning rate was 1.5 Hz.

SFE Measurements. Contact-angle measurements of neat films were applied to estimate the film surface free energy (SFE), wherein deionized water (θ_{water}) and Diiodomethane (θ_{CH2I2}) were employed as the calibrated liquids.

Supplementary Figures

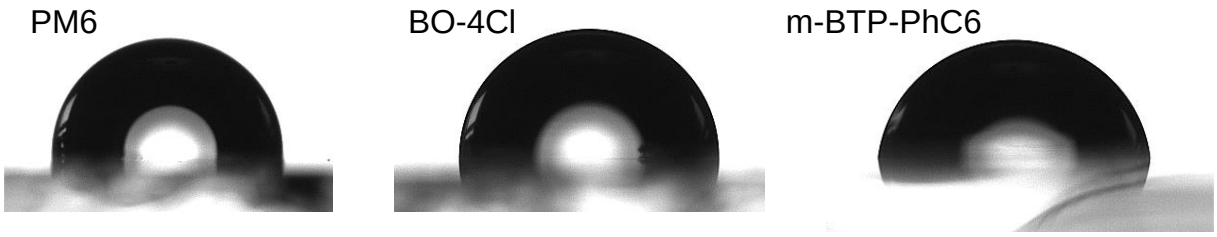

Figure S1. Water contact-angles of different materials. Water contact-angles of PM6, BO-4Cl, and m-BTP-PhC6. Form Table S1, Iondon dispersion (γ_d), and polar (γ_p) component values are shown, with an SFE value of 30.50, 40.22, and 37.87 mJ cm^{-2} for pure PM6, m-BTP-PhC6, and BO-4Cl neat films, respectively. Flory-Huggins interaction parameter (χ) based on the surface free energy (SFE) of above materials was calculated, according to the formula, $\chi_{D,\ A}=K\left(\sqrt{\gamma_D}-\sqrt{\gamma_A}\right)^2$.

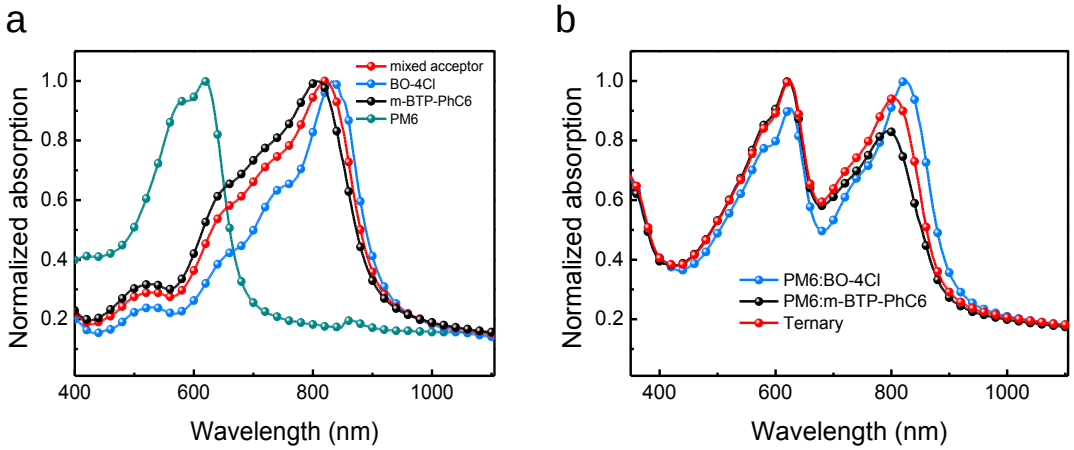

Figure S2. The normalized absorption. (a) PM6, m-BTP-PhC6, and BO-4Cl and mixed acceptor (0.3:0.7 wt%) blends. (b) PM6:BO-4Cl, PM6: m-BTP-PhC6 and ternary blends (1:0.36:0.84 wt%).

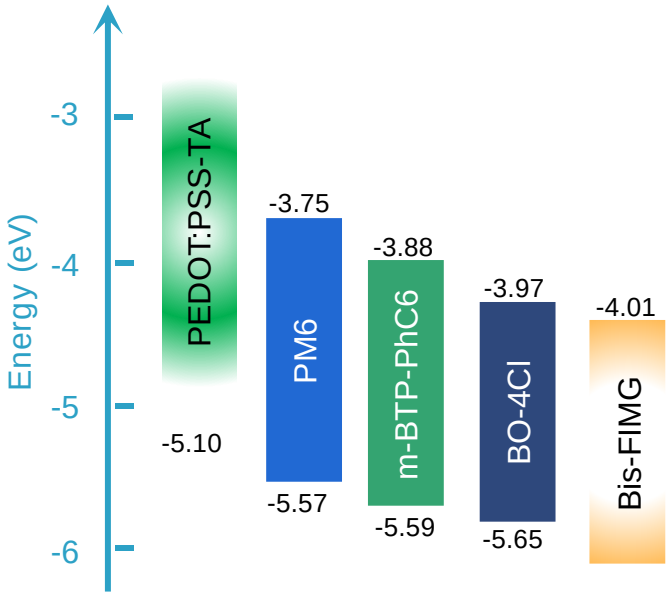

Figure S3. Energy level diagram of the studied materials.

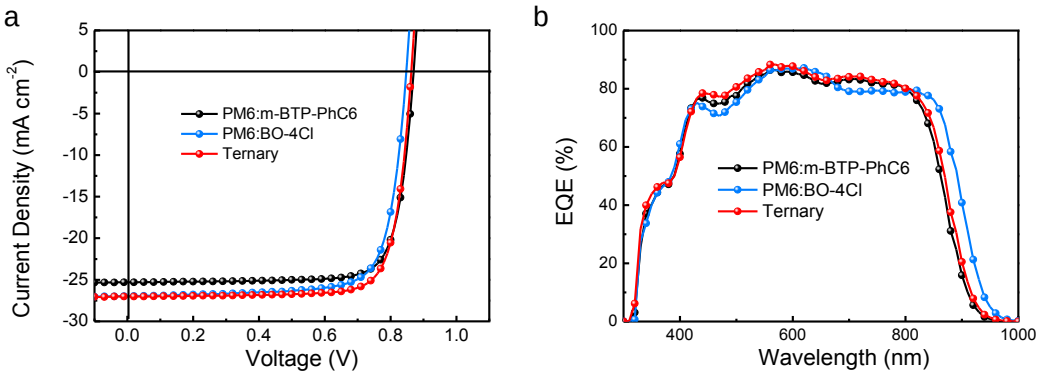

Figure S4. Photovoltaic performance of OSCs with pristine PEDOT:PSS HTL. (a) *J-V* curves of the binary and ternary OSCs. (b) EQE curves of the corresponding OSCs.

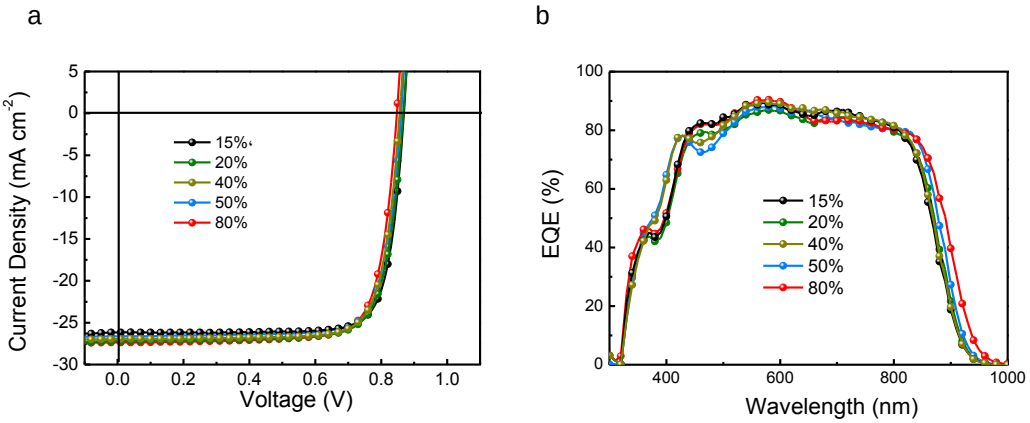

Figure S5. Photovoltaic performance of the ternary OSCs with TA- PEDOT:PSS HTL. (a) *J-V* curves of the ternary OSCs with the varied ratio of BO-4Cl in the acceptor components (wt%). (b) EQE curves of the corresponding OSCs.

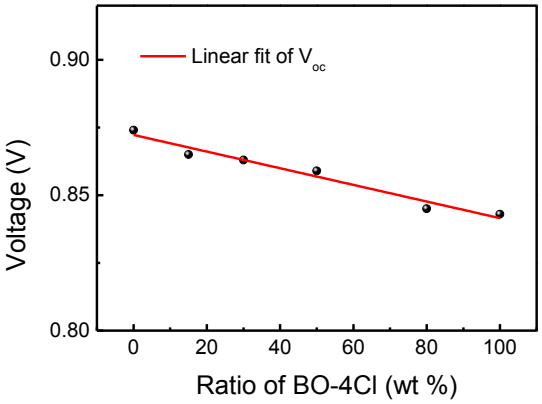

Figure S6. The linear relationship between voltage and the ratio of BO-4Cl in the acceptors for ternary OSCs.

中 国 计 量 科 学 研 究 院

报告编号 GXgf2021-12062
Report No.

测 试 结 果
Test Results

有效面积 (mm^2)	短路电流 I_{sc}(mA)	开路电压 V_{oc}(V)	最大功率 P_{max}(mW)
5.979	1.617	0.857	1.092
最大功率电流 I_{max}(mA)	最大功率电压 V_{max}(V)	填充因子 FF (%)	转换效率 η (%)
1.476	0.740	78.8	18.3

注 Note:
1. 测试所用 mask（2#M3）的面积为 5.979 mm^2（证书编号：CDjc2020-00241）。
The mask (2#M3) area is 5.979 mm^2 (Certificate No.: CDjc2020-00241).
2. 此数据仅对被测样品当时状态有效。
The data apply only at the time of the test for the sample.
3. 英文证书摘要见附录。
Summary of certificate in English is attached in the appendix.

----------以下空白----------

声明 Statement：
1. 我院仅对加盖“中国计量科学研究测试专用章”的完整报告负责。
NIM is ONLY responsible for the complete report with the test stamp of NIM.
2. 本报告的测试结果仅对所测试的样品有效。
The report is ONLY valid for the tested sample or instrument.
3. 本报告用中英文两种语言表达，准确含义以中文为准。
The report is expressed in both English and Chinese, with the Chinese version as standard.

测 试 员： 核 验 员：
Tested by Checked by

2019-cs-R0520

第 4 页 共 4 页

Figure S7. Certification of the ternary device was measured as 18.3% at the National Institute of Metrology (NIM), Beijing, China.

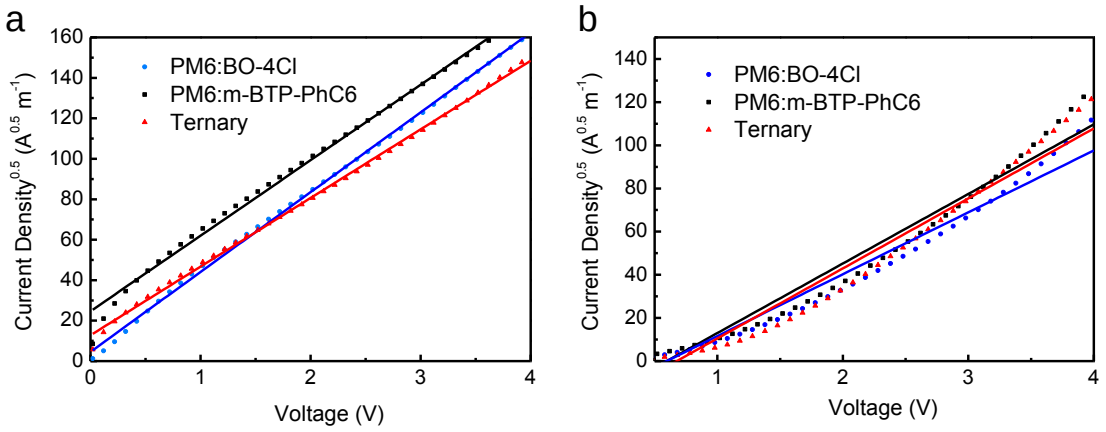

Figure S8. $J^{0.5}$-V curves of the (a) hole-only devices and (b) electron-only devices based on binary and ternary blends. Hole-only devices with a structure of ITO/PEDOT: PSS-TA/active layer/MoO_3/Ag and electron-only devices with a structure of ITO/ZnO/active layer/Bis-FIMG/Ag. PM6: m-BTP-PhC6 binary BHJs display hole and electron mobilities (μ_h and μ_e), μ_h of 2.92×10^{-4} cm^2 V^{-1} S^{-1} and μ_e of 1.77×10^{-4} cm^2 V^{-1} S^{-1}, with μ_h/μ_e value of 1.64. Ternary BHJs with PM6:m-BTP-PhC6: BO-4Cl (30 wt%) exhibit μ_h of 3.12×10^{-4} cm^2 V^{-1} and μ_e of 2.18×10^{-4} cm^2 V^{-1} S^{-1}, with μ_h/μ_e value of 1.43.

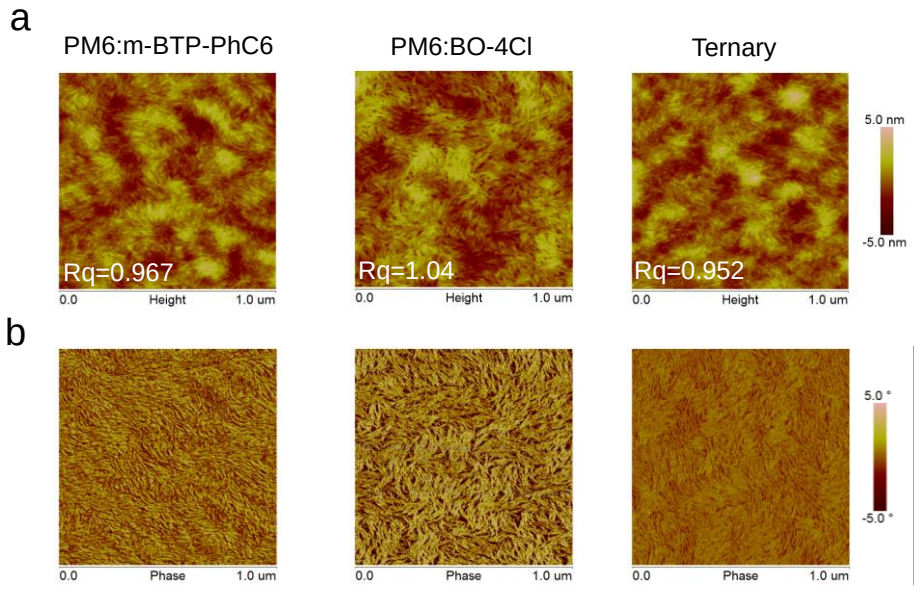

Figure S9. Morphology characteristics of binary and ternary films. (a) AFM height and (b) phase images of blends of the ternary and binary blend. Smooth surface morphologies are generally observed in binary and ternary films by atomic force microscopy (AFM), with root-mean-square surface roughness (R_q) values of

0.967 nm (PM6:m-BTP-PhC6), 1.04 nm (PM6:BO-4Cl), and 0.952 nm (PM6:m-BTP-PhC6:BO-4Cl), respectively.

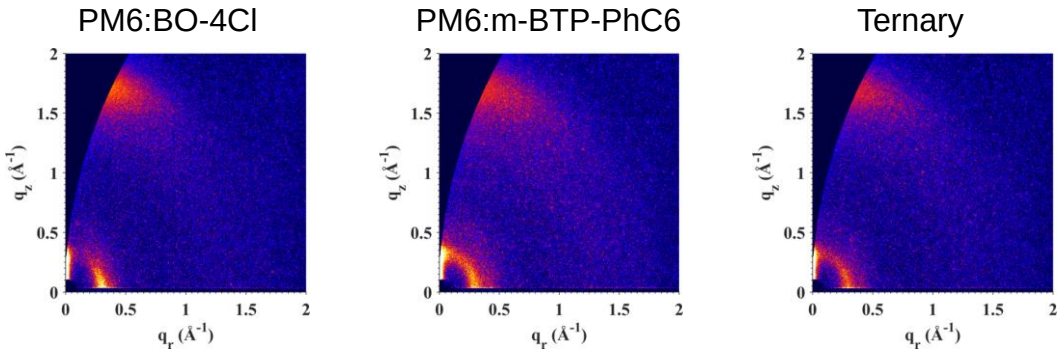

Figure S10. 2D GIWAXS measurements. The crystallinity and molecular orientation of binary and ternary films were studied by GIWAXS. By introducing BO-4Cl into the PM6: m-BTP-PhC6 system, the ternary blends show a lamellar peak at q_r = 0.316 Å^{-1} (d = 19.9 Å) and a π-π stacking peak at q_z = 1.72 Å^{-1} (d = 3.65 Å), which are similar to those of PM6: m-BTP-PhC6 binary blends. At the same time, adding only 30% BO-4Cl to fabricate ternary film, the intensity of the π-π peak at 1.72 Å^{-1} is kept, while the peak at qz = 0.316 Å^{-1} decreased.

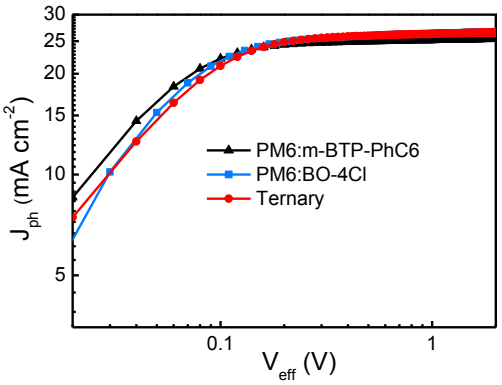

Figure S11. The relationship between effective voltage (V_{eff}) and photocurrent density (J_{ph}) was investigated and show that the ratios of J_{sc}/J_{sat} (note J_{sat} is saturation photocurrent density at V_{eff} of 2.5 V) are 98.3%, 98.0%, and 98.8%, for PM6: m-BTP-PhC6, PM6:BO-4Cl, and PM6: m-BTP-PhC6:BO-4Cl ternary blend, respectively. These values indicate the ternary devices possess high probabilities of exciton dissociation.

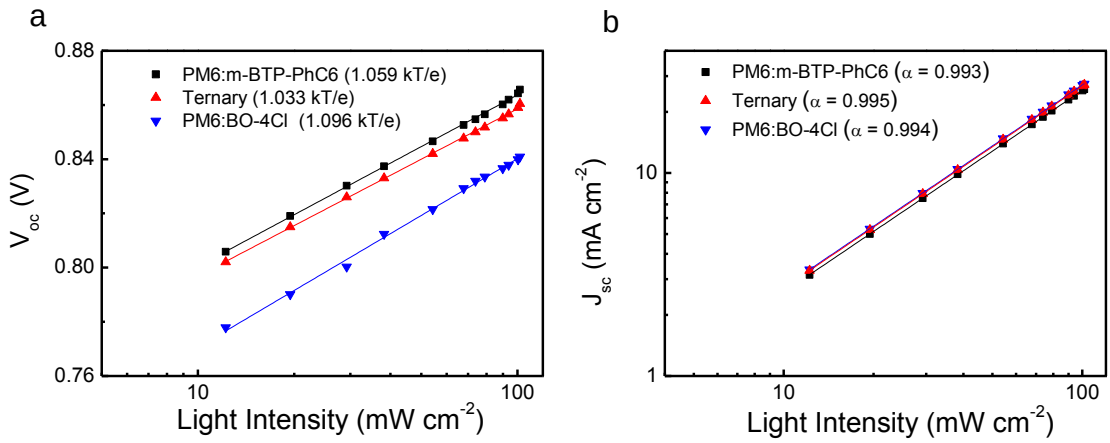

Figure S12. Excitonic recombination of ternary and binary devices. The dependence of (a) V_{oc} and (b) J_{sc} versus light intensity (P_{light}) for binary and ternary devices, as the slopes from 1.059 KT/e (binary) to 1.033 kT/e (ternary) and α form 0.993 (binary) to 0.995 (ternary).

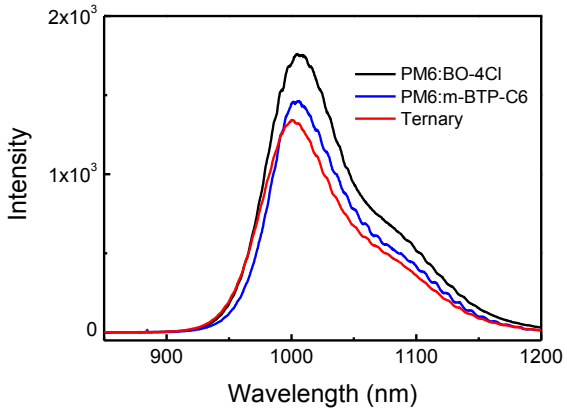

Figure S13. Steady PL spectra of the corresponding blend films excited at 700 nm.

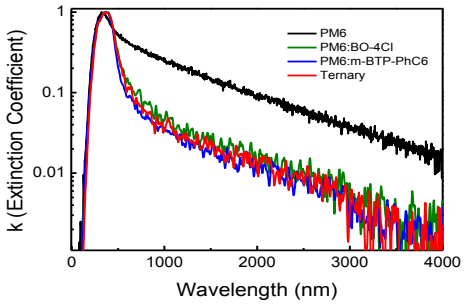

Figure S14. Time-Resolve Photoluminescence spectra (excited at 515 nm) of different films. Obviously, the ternary blend (τ: 89.32 ± 2.37 ps) has also faster rate than those of binary blends (τ: 95.71 ± 2.93 ps for PM6:BO-4Cl, and τ: 93.64 ± 2.55 ps for PM6: m-BTP-PhC6).

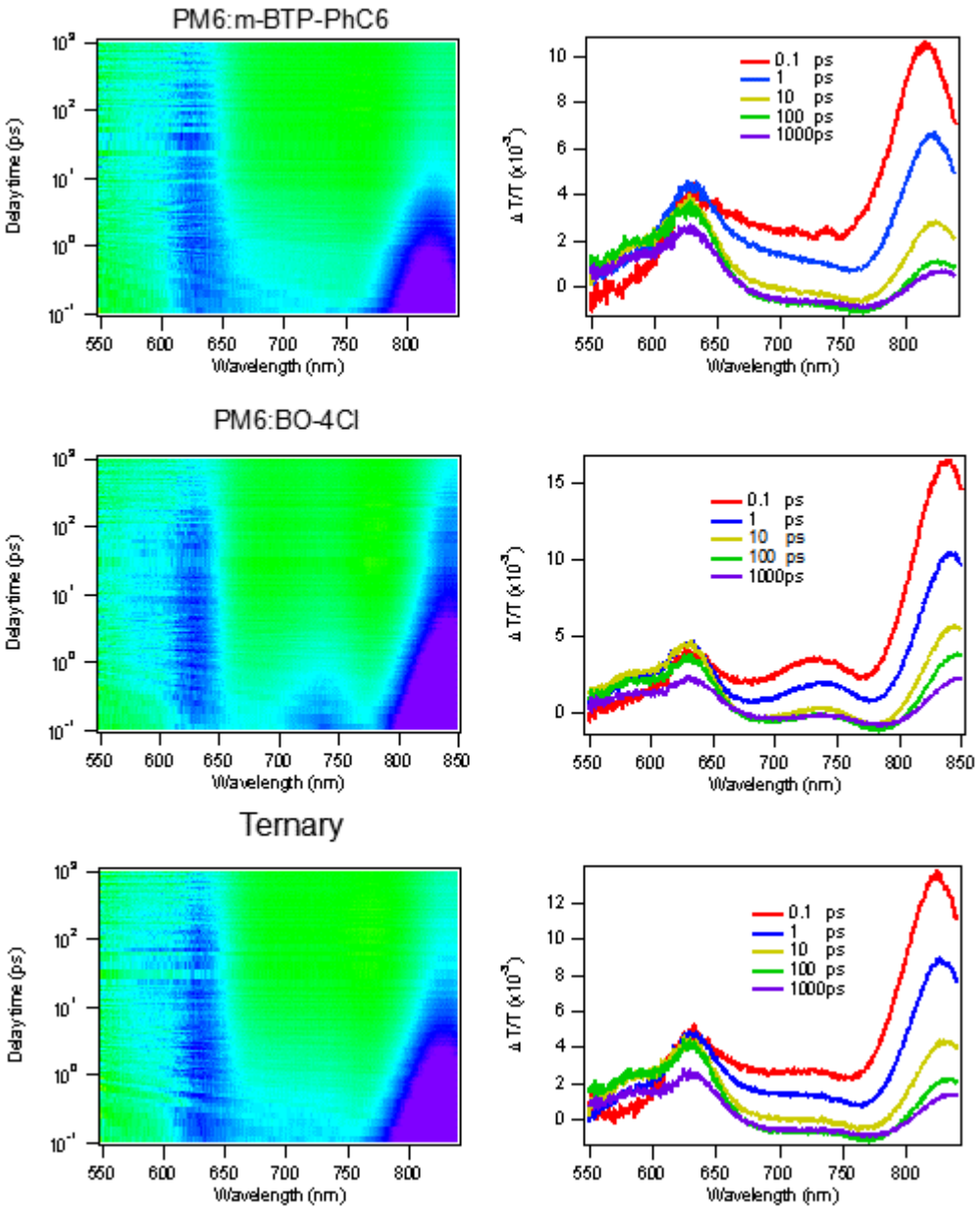

Figure S15. TA measurements. Herein, we selected 750 nm to pump acceptors only without exciting donors due to the good separation of the absorption of donor and acceptors. The bleach peak at ~830 nm appears in both PM6:m-BTP-PhC6 binary and ternary blend films, corresponding to the stimulated emission (SE) and ground-state bleach (GSB) of the absorption transition in m-BTP-PhC6 due to photoexcitation. The representative color plot of the fs-TA spectra of the ternary BHJ under 750 nm excitation with a fluence below 10 mJ cm^{-2}.

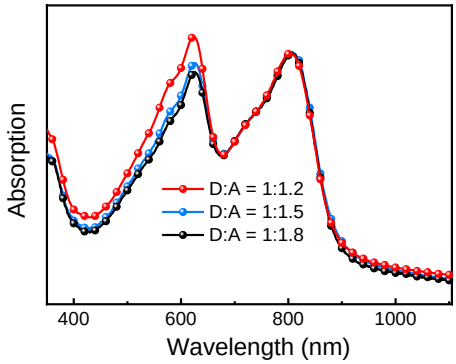

Figure S16. The normalized absorption (to 805 nm) of ternary blends with different D/A ratios.

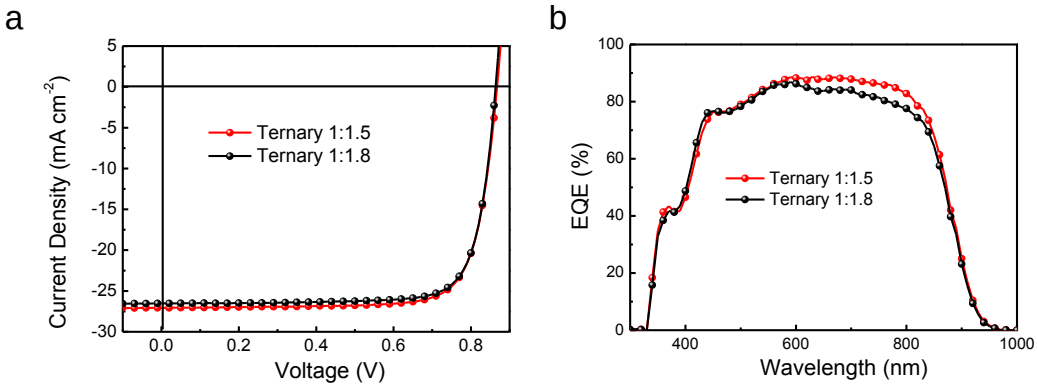

Figure S17. Photovoltaic performance of the devices. (a) *J-V* curves of the ternary OSCs with the varied ratio of the donor to acceptor. (b) EQE curves of the corresponding OSCs.

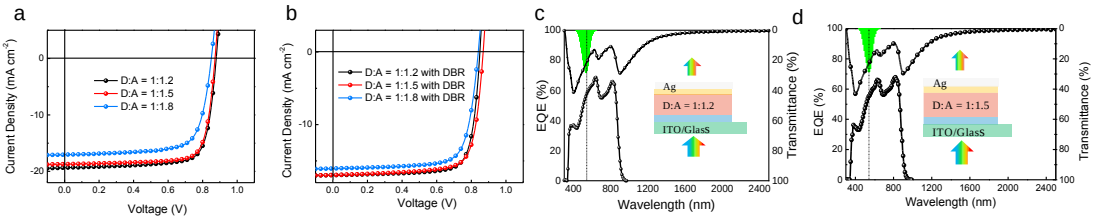

Figure S18. Photovoltaic performance. *J-V* curves of the ternary OSCs with different D/A ratios (a) without DBR and (b) with DBR. (c-d) Transmittance and EQE spectra of the device with different D/A ratios without DBR.

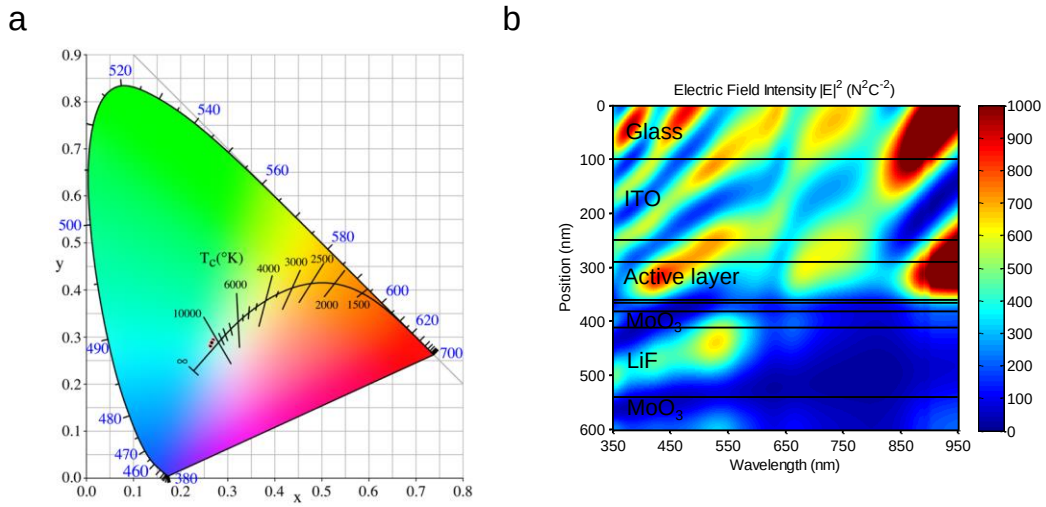

Figure S19. CIE coordinates for STOSCs and Simulated $|E|^2$ distribution. (a) STOSC (D/A=1:1.2) is at (0.264, 0.282); STOSC (D/A=1:1.5) is at (0.267, 0.288); STOSC (D/A=1:1.8) is at (0.269,0.293). (b) Simulated $|E|^2$ distribution of D-STOSC (D/A=1:1.5 with DBR).

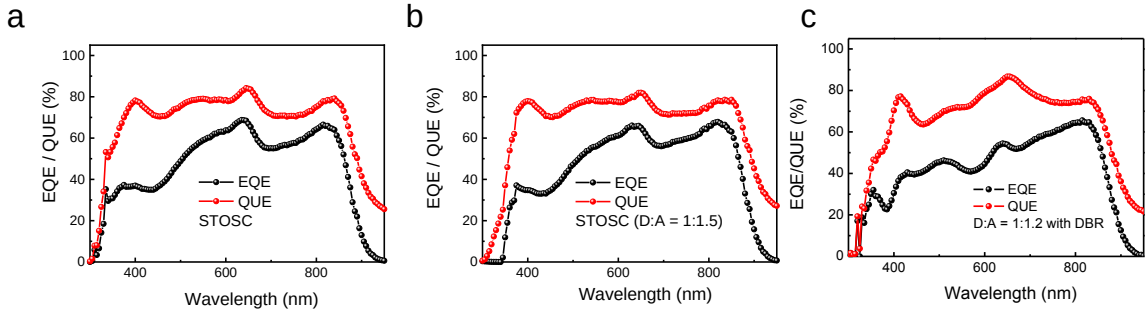

Figure S20. EQE and QUE of the different devices. (a) STOSC (D:A = 1:1.2 without DBR), (b) STOSC (D:A = 1:1.5 without DBR) and (c) D-STOSC (D:A = 1:1.2 with DBR). The EQE(λ) values of ST-OSCs are similar to the *JV* test. QUE is obtained by the sum of EQE and transmittance (T), defined as QUE(λ) = EQE(λ) + T(λ).

Figure S21. Certification report. Certification report measured at the Chinese National Photovoltaic Industry Metrology and Testing Center (NPVM), Fujian Metrology Institute, China.

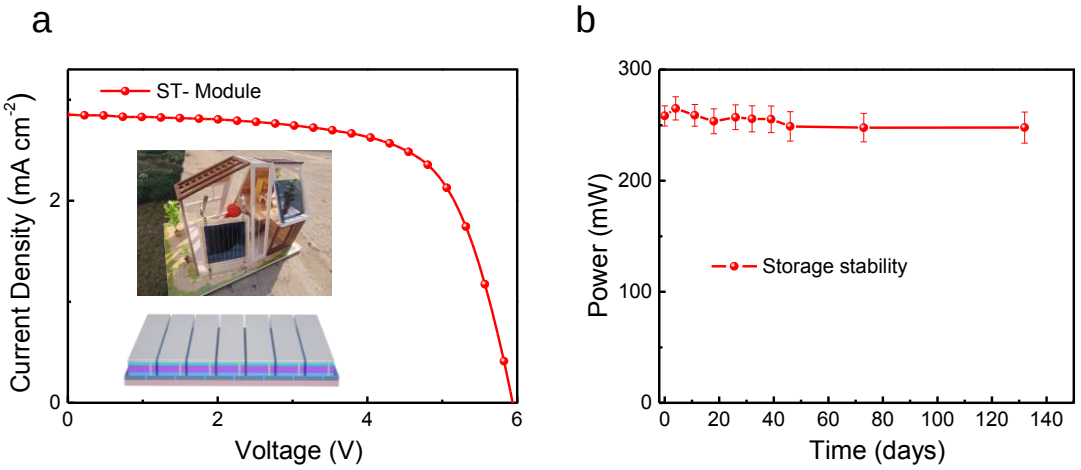

Figure S22. (a) The *J–V* characteristics of semitransparent modules and power-generating windows of model building (left: opaque module, and right: semitransparent module). (b) The performance of encapsulated organic solar modules under indoor storage. The average values with standard deviation are obtained from 7 modules.

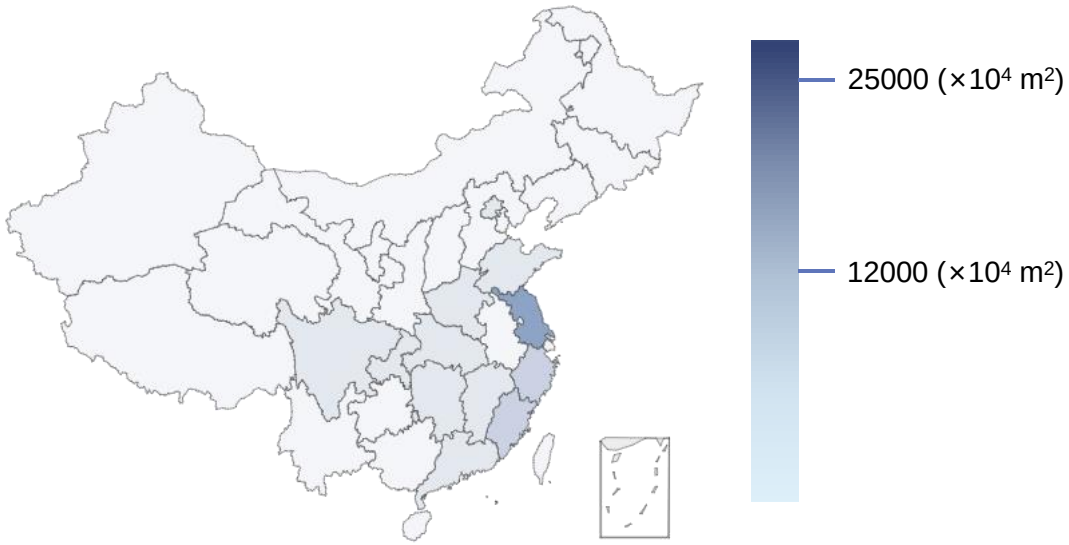

Figure S23. The simulated total number of window glass in new buildings across China.

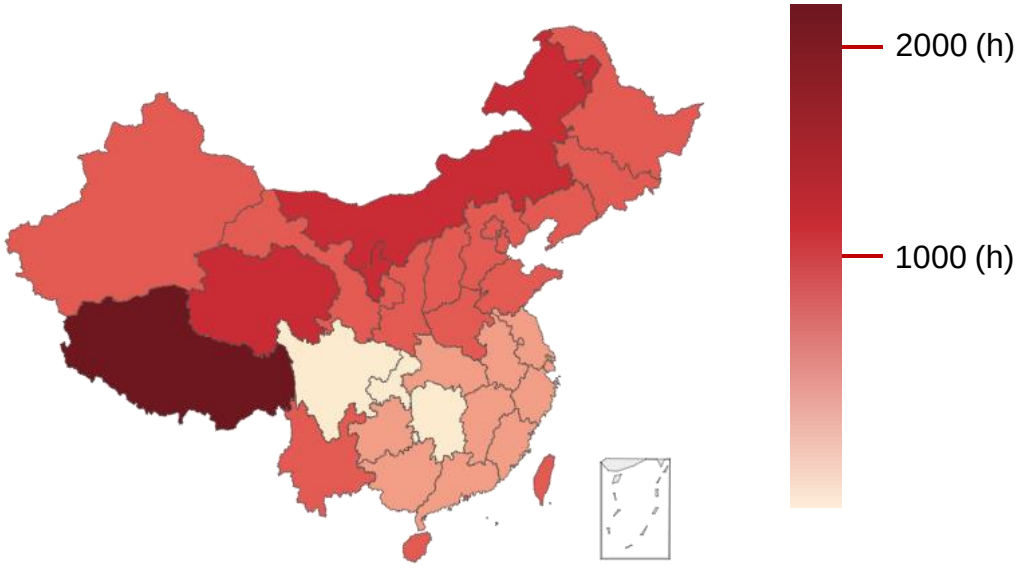

Figure S24. The average annual effective sunlight time across China.

Supporting Tables

Table S1. Surface free energy characteristics of the neat films.

Parameter	PM6	BO-4Cl	m-BTP-PhC6	BO-4Cl: m-BTP-PhC6
θ_{water} [deg]	96.05	92.68	87.26	87.64
θ_{CH2I2} [deg]	56.70	43.75	38.79	43.03
γ^d [mJ cm $^{-2}$]	29.48	37.10	38.58	36.17
γ^p [mJ cm $^{-2}$]	1.02	0.77	1.64	1.89
SFE γ [mJ cm $^{-2}$]	30.50	37.87	40.22	38.06
$X_{D,A}$	-	0.398	0.671	0.035

Table S2. Photovoltaic performance of binary and ternary OSCs.

Active Layer[a]	V_{oc} (V)	J_{sc} (mA cm^{-2})	$J_{calc.}$ (mA cm^{-2})[b]	FF (%)	PCE (%)[c]
PM6: m-BTP-PhC6	0.876 (0.884±0.002)	25.27 (25.32±0.19)	25.24	79.83 (79.42±0.26)	17.65 (17.32±0.11)
PM6: BO-4Cl	0.845 (0.843±0.003)	27.18 (27.22±0.31)	26.86	77.64 (76.35±0.92)	17.83 (17.61±0.21)
Ternary	0.868 (0.865±0.003)	26.99 (27.07±0.17)	26.83	79.49 (79.04±0.39)	18.61 (18.38±0.06)
Ternary[d]	0.857	27.04	-	78.80	18.30

[a] Active layers with the total donor: acceptor ratio of 1:1.2 wt%. [b] Integrated current densities from the EQE curves. [c] Averaged values in the parenthesis form 15 devices. [d] Ternary OSCs certified at the National Institute of Metrology (NIM), Beijing.

Table S3. Photovoltaic performance of ternary OSCs with pristine PEDOT:PSS HTL.

Active Layer[a]	V_{oc} (V)	J_{sc} (mA cm^{-2})	$J_{calc.}$ (mA cm^{-2})[b]	FF (%)	PCE (%)[c]
PM6: m-BTP-PhC6	0.870 (0.870±0.003)	25.28 (25.13±0.14)	25.54	79.76 (79.31±0.17)	17.54 (17.22±0.31)
PM6: BO-4Cl	0.847 (0.846±0.002)	26.96 (26.85±0.29)	26.33	76.90 (76.71±0.24)	17.55 (17.41±0.30)
Ternary	0.863 (0.861±0.005)	27.00 (26.89±0.14)	26.85	79.31 (79.40±0.32)	18.43 (18.25±0.13)

[a]Active layers while keeping total donor: acceptor ratio as 1:1.2, wt%. [b] Integrated current densities from the EQE curves. [c] Averaged values in the parenthesis form 10 devices.

Table S4. Photovoltaic performance of binary and ternary OSCs with PEDOT:PSS-TA for HTL.

Active Layer[a]	V_{oc} (V)	J_{sc} (mA cm^{-2})	$J_{calc.}$ (mA cm^{-2})[b]	FF (%)	PCE (%)[c]
0%	0.876 (0.884±0.002)	25.27 (25.32±0.19)	25.24	79.83 (79.42±0.26)	17.65 (17.32±0.11)
15%	0.869 (0.875±0.003)	26.16 (26.20±0.20)	25.68	80.66 (80.06±0.49)	18.31 (18.12±0.19)
20%	0.869 (0.872±0.002)	26.44 (26.55±0.21)	26.24	79.43 (79.88±0.22)	18.28 (18.11±0.10)
30%	0.868 (0.865±0.003)	26.99 (27.07±0.17)	26.83	79.49 (79.04±0.39)	18.61 (18.38±0.06)
40%	0.858 (0.863±0.001)	26.88 (26.91±0.03)	26.48	78.80 (79.11±0.15)	18.17 (18.03±0.31)
50%	0.861 (0.859±0.002)	26.62 (26.54±0.21)	26.45	79.12 (78.91±0.29)	18.13 (17.99±0.22)
100%	0.845 (0.843±0.003)	27.18 (27.22±0.31)	26.86	77.64 (76.35±0.92)	17.83 (17.61±0.21)

[a] Active layers with the varied BO-4Cl weight ratio in the acceptor components (wt%) while keeping total donor: acceptor ratio as 1:1.2 wt%. [b] Integrated current densities from the EQE curves. [c] Averaged values in the parenthesis form 15 devices.

Table S5. Hole and electron mobilities of different devices from SCLC measurements.

Sample	μ_h ($\times10^{-4}$ cm^2 V^{-1} S^{-1})	μ_e ($\times10^{-4}$ cm^2 V^{-1} S^{-1})	μ_h/μ_e
PM6:BO-4Cl	4.05±0.38	2.16±0.38	1.87
Ternary (80%)	3.92±0.64	1.99±0.33	1.96
Ternary (30%)	3.12±0.41	2.18±0.26	1.43
Ternary (20%)	3.11±0.55	2.21±0.26	1.41
PM6:m-BTP-PhC6	2.92±0.64	1.77±0.16	1.64

Table S6. Photovoltaic performance of ternary OSCs.

Active Layer[a]	V_{oc} (V)	J_{sc} (mA cm^{-2})	$J_{calc.}$ (mA cm^{-2})[b]	FF (%)	PCE (%)[c]
1:1.5	0.869 (0.866±0.002)	27.06 (26.62±0.22)	26.40	78.31 (78.81±0.93)	18.32 (18.10±0.18)
1:1.8	0.864 (0.863±0.002)	26.52 (26.61±0.17)	25.51	79.41 (76.97±3.02)	18.13 (17.63±0.70)

[a] Donor: acceptor ratio, wt%. [b] Integrated current densities from the EQE curves. [c] Averaged values in the parenthesis form 10 devices.

Table S7. Photovoltaic performance of ternary OSCs with different D/A ratio.

D/A ratio	V_{oc} (V)	J_{sc} (mA cm^{-2})	$J_{calc.}$ (mA cm^{-2})[c]	FF (%)	PCE (%)[d]	AVT (%)	CRI	IRR
1:1.2[a]	0.878 (0.875±0.003)	19.35 (19.04±0.11)	18.46	76.90 (77.10±0.22)	13.05	19.32	73	0.88
1:1.2[b]	0.868 (0.864±0.003)	16.98 (17.21±0.13)	16.44	76.34 (75.32±0.22)	11.26	29.71	90	0.89
1:1.5[a]	0.872 (0.865±0.002)	18.72 (18.21±0.13)	18.33	78.44 (77.45±0.17)	12.78	21.00	73	0.88
1:1.5[b]	0.849 (0.851±0.003)	16.96 (17.33±0.25)	16.24	78.24 (77.53±0.26)	11.18	32.07	90	0.90
1:1.8[a]	0.851 (0.844±0.003)	17.04 (17.15±0.20)	17.13	73.29 (74.02±0.31)	10.62	23.37	73	0.87
1:1.8[b]	0.840 (0.842±0.004)	16.06 (16.15±0.30)	15.83	75.26 (74.21±0.15)	10.15	35.72	89	0.87

[a] ST-OSC without DBR. [b] ST-OSC with DBR. [c] Integrated current densities from the EQE curves. [d] Averaged values in the parenthesis form 10 devices.

Table S8. Photovoltaic performance of opaque and semitransparent modules.

Thickness of Ag	V_{oc} (V)	J_{sc} (mA cm^{-2})	FF (%)	PCE (%)
150 nm	6.02 (6.04±0.02)	3.70 (3.62±0.15)	72.08 (71.11±0.30)	16.04 (15.72±0.22)
150 nm[a]	6.06 (6.04±0.01)	3.56 (3.59±0.04)	71.63 (71.07±0.60)	15.46 (15.39±0.08)
16 nm	5.91	2.83	67.45	11.28

[a] Results was measured by the Chinese National Photovoltaic Industry Metrology and Testing Center (NPVM), also see experimental section.

Energy model analysis:

1. Annual new building area: S_{total}
2. Window glass coverage in the new building: α
3. The total area of window glass in the new building: S_{glass}

$$S_{glass} = \alpha \times S_{total} \quad (1)$$

4. Annual effective sunlight time: $T_{sunlight}$
5. Output power per unit area of power window: $P_{output\ power}$ $(at\ 100\ W/m^2)$
6. The energy generation for photoelectric conversion ($E_{genaration}$):

$$E_{genaration} = S_{glass} \times P_{output\ power} \times T_{sunlight} \quad (2)$$

7. Annual energy saving per unit area: $P_{insulation}$ $(at\ 50\ kWh/m^2)$
8. Annual energy saving from IR reflection of heat dissipation (E_{saving}):

$$E_{saving} = P_{insulation} \times S_{glass} \quad (3)$$

9. Annual total energy gain ($E_{Total\ energy\ gain}$) is equal to the sum of energy-saving from IR reflection of heat dissipation (E_{saving}) and photoelectric energy generation ($E_{genaration}$) :

$$E_{Total\ saved\ gain} = E_{saving} + E_{genaration} \quad (4)$$

Description:

1. The numbers of annual new building area (S_{total}) of 34 provinces and cities in China at 2019 are obtained from the China National Bureau of Statistics (http://www.stats.gov.cn/).
2. Window glass coverage in new building (α) is assigned as the value of 0.15 at the middle bar for the ratio of glazing to floor area, according to Standard for daylighting design of buildings, Ministry of housing and urban rural development of China (http://mohurd.gov.cn/).
3. Annual energy saving per unit area ($P_{insulation}$) of power windows is assigned as 50 kWh/m^2 at the low bar of energy saving in China, which is extracted from data that indicates energy saving of Low-E glass consisting of thin metal and metal oxide layout over that of common architectural glass. For instance,
    1) Annual energy saving per unit area of 220 ~ 240 kWh/m^2 at Beijing, north part of

China, Energy and Buildings 206, 109570 (2020);

2) Annual energy saving per unit area of 250-300 kWh/m^2 at Hebei in China (Energy-Saving Analysis of LOW-E glass in Jinan Region, Hebei University of Engineering, 2012)
3) Annual energy saving per unit area of 130-200 kWh/m^2 at Chongqing in China (Study on Energy Saving of Low-E Glass in Chongqing, Chongqing University, 2007)
4) Annual energy saving per unit area around 30 kWh/m^2 at Guangdong in China (Study on Energy Saving of Low-E Glass in Residential Buildings in the Subtropical Region, Guangdong University of Technology, 2012)
5) Annual energy saving per unit area on 3M window films around 200 kWh/m^2 in USA (https://multimedia.3m.com/mws/media/1145162O/3m-commercial-window-film-energy-efficiency-brochure.pdf).

4. Note that ST-OSCs consisting of thin silver and with the distributed Bragg reflector with IRR of 0.90 is superior to that of regular IR reflection films.
5. Assumption of output power per unit area of power window at 100 W/m^2 with PCE of 10% under AM1.5 illumination, and without consideration of the influence of exceptional weather.